

Model for the dynamics of the large-scale circulations in two-layer turbulent convection

Yu Sun,¹ Yi-Chao Xie,² Jin-Xiao Xie^{1b},³ Jin-Qiang Zhong^{1b},^{1,3,*}
Jianwei Zhang,^{1,†} and Ke-Qing Xia^{4,‡}

¹*School of Physics Science and Engineering, Tongji University, Shanghai 200092, China*

²*State Key Laboratory for Strength and Vibration of Mechanical Structures and School of Aerospace, Xi'an Jiaotong University, Xi'an 710049, China*

³*Department of Aeronautics and Astronautics, Fudan University, Shanghai 200433, China*

⁴*Center for Complex Flows and Soft Matter Research and Department of Mechanics and Aerospace Engineering, Southern University of Science and Technology, Shenzhen 518055, China*



(Received 21 December 2023; accepted 27 February 2024; published 22 March 2024)

We present a physically motivated low-dimensional model for the dynamics of two interacting large-scale circulations (LSC) in two-layer turbulent convection. Inspired by our experimental results of the flow dynamics and coupling in two-layer turbulent convection [J. Fluid Mech. **728**, R1 (2013)], the model extends previous studies of single-LSC dynamics to incorporate four stochastic ordinary differential equations describing the strength δ and azimuthal orientations θ of two vertically aligned LSCs. The interaction terms of the two LSCs, i.e., thermal and viscous coupling terms, are predicted based on the influence of the fluid temperature by the other LSC through heat advection and thermal diffusion, and the enhanced (reduced) viscous damping across the interface between the two LSCs. Our model produces two stable LSC rolls and predicts their preferred flow states for the thermal and viscous couplings. The model describes properly the diffusive motion of both δ and θ of the two LSCs, and the Poissonian distribution of time interval between LSC cessations. More importantly, our study reveals that flow reversals and cessations in two-layer convection can be achieved when turbulent fluctuations drive the azimuthal diffusion of the two LSCs into a flow state that the two LSC planes are orthogonal to each other, the strength of the LSC in the fluid layer with a relatively larger Rayleigh number reduces to zero deterministically, owing to the unbalanced buoyancy forcing. Our model provides accurate predictions for the enhanced occurrence frequency of flow reversals observed in the experiment, and it suggests a new dynamical process of flow reversals in multilayer turbulent convection.

DOI: [10.1103/PhysRevFluids.9.033501](https://doi.org/10.1103/PhysRevFluids.9.033501)

I. INTRODUCTION

Turbulent thermal convection represents many important features of natural flows. It is found widely in oceans and atmosphere [1], in the Earth's liquid core [2], in the interior of terrestrial planets [3] and the outer layer of the Sun [4]. In many geophysical and astrophysical settings, turbulent convection often occurs in multilayers, examples include multilayer convection in gas-giant planets [5], thermal-driven or density-driven flows in the coupled system of oceanic and atmospheric

*jinqiang@fudan.edu.cn

†zhang@tongji.edu.cn

‡xiakq@sustech.edu.cn

convection [1], and convection at the boundary of the Earth's lower mantle and the outer core [6]. It is also related to many industrial processes such as liquid-encapsulated crystal growth [7]. Exploring the fluid dynamics of multilayer turbulent convection may assist us to understand a wide variety of natural phenomena, and is of fundamental research interest in science and engineering.

In Rayleigh-Bénard convection (RBC), a paradigmatic model for studying turbulent thermal convection in laboratory, a fluid layer confined between two horizontally parallel plate is heated from below and cooled from above to generate buoyancy-driven flows [8–10]. For a given geometry of the convection cell, the convection flows in RBC are determined by two nondimensional parameters. The Rayleigh number $Ra = \alpha g \Delta T H^3 / \kappa \nu$ representing the buoyancy forcing, and the Prandtl number $\sigma = \nu / \kappa$ characterizing fluid properties, where α , κ and ν are, respectively, the isobaric thermal expansion coefficient, thermal diffusivity and kinematic viscosity of the fluid, g is gravitational acceleration, ΔT is temperature difference across the fluid layer. The cell geometry is described by its symmetry and aspect ratio $\Gamma = D/H$, where H and D are the vertical and horizontal dimensions of the convection cell, respectively.

When the Rayleigh number is sufficiently high in RBC, various kinds of coherent flow structures arise and the large-scale circulation (LSC) is one of the most salient one. LSC forms in the background of turbulence, consisting of self-organized thermal plumes emanating from the thermal boundary layers (BLs), which has enlivened experimental and theoretical studies in turbulent convection until now (see, e.g., Refs. [11–26]). In cylindrical cells of aspect ratio 1, the LSC appears as a single convection roll that oriented nearly vertically with the upflow and the downflow on opposite sides of the cell. A rich variety of dynamics of the LSC has been reported in laboratory experiments, including spontaneous meandering of the LSC azimuthal orientation θ_0 and its oscillations that manifest as twisting and sloshing modes [14,15,20]. The flow strength δ of the LSC fluctuates around a stable point while occasionally drops to zero abruptly, i.e., the roll structure vanishes suddenly, and then the flow will restart at any orientation, which is known as cessation events [27,28]. Because of the rotational invariance of the cylindrical geometry, any azimuthal orientation θ_0 is an equally effective state for the quasi-2D LSC structure [28]. Therefore, after a cessation event the LSC undergoes a change of azimuthal orientation with random amplitude (reorientation). Reversal is a particular kind of dynamic event during which the LSC orientation θ changes by π [29,30]. It can be achieved by rotations of the LSC plane without an obvious change in flow strength δ , or by cessation when the flow structure vanishes and restarts at quite opposite direction. Flow reversals are believed to be associated with many important phenomena in geophysical scale, such as the reversal of the geomagnetic field, and changes of the wind directions in the atmosphere.

Theoretical models have been developed to interpret the LSC dynamics in turbulent RBC and to make predictions for plenty of the observed phenomena. Rooted in the Navier-Stokes (NS) equation, a low-dimensional model consisting two stochastic ordinary equations respectively describing LSC strength and its azimuthal motion was proposed [18,19]. This model describes the diffusive behavior of the LSC flow strength as stochastic motion in a potential well, and reproduces successfully the observed phenomenon of LSC in leveled [19] or tilted [25] cylinder container, such as the meandering, cessations, and reversals. Other phenomenological models are devoted to describe the stochastic [13,16] and deterministic [17,31] nature of LSC reversals in RBC.

Despite the intensive studies of the LSC dynamics in a single-roll configuration, relatively fewer works are devoted to investigate multiple-roll flow dynamics in turbulent convection. In RBC systems when the aspect ratio Γ deviates from 1, one observes that the single-roll structure of the LSC breaks down and multiple convection rolls can be generated. For instance, vertically lined-up multiple rolls form in convection cells with Γ smaller than one [32–36]. In cylindrical cells with $\Gamma = 0.5$ two different states of convection can coexist, i.e., single-roll state and double-roll state. In the state of double-roll convection, the two rolls are often found in a viscous-coupling mode in which the fluid velocities of two LSCs are in the same direction at the midheight where they meet [32,33]. Horizontally lined-up multiple rolls are observed in convection cells with large aspect ratios [37–39]. For instance, in a rectangular cell with $\Gamma = 4$ it is reported that two counterrotating LSCs are laid out horizontally [38]. Their flow directions at the cell center are both ascendent

and descendent depending on the applied temperature difference across the fluid cell. However, two corotating, horizontally adjacent rolls can also form, with prominent fluctuation in their flow strength and circulation path [37]. The interaction of two neighboring LSCs is examined in a convection cell consisting two horizontally connected cubic containers [26,40]. The competition of thermal and viscous forcing in between the two LSCs results in bistable flow orientations, where the two circulating rolls can be found both in a corotating and counterrotating state. Motivated by these experimental findings a theoretical model is proposed to account for the coupling dynamics of the two interacting LSCs, which provides predictions of the azimuthal orientations and flow strengths of the two LSCs in good agreement with the experiment.

In a recent experimental study Xie and Xia [41] investigate the dynamics of two vertically aligned LSCs in a cylindrical cell filling with two immiscible fluids. They reported that the two LSC rolls have two preferred azimuthal orientations separated by π . Two dynamic modes, thermal coupling and viscous coupling, are identified as the preferred flow configurations. Remarkably, it is observed that in the lower fluid layer with a relatively higher Ra, cessation events occur much more frequently than in single-layer turbulent convection, and a significant portion of cessations end up as reversals. In the upper fluid layer that has a lower Ra, however, the stochastic fluctuations of the LSC strength is largely suppressed and cessation events are hardly present. The underlying mechanism responsible for the observed enhanced/suppressed LSC cessations and reversals remains elusive. The heat transport efficiency as a function of the layer thickness ratio in two-layer turbulent convection is studied [42]. When the layer ratio is not too small or too large, both layers are found to have large-scale convection rolls. The heat transport efficiency in this regime is insensitive to the change in the layer ratio. However, when one layer is thin enough to have a Rayleigh number below the onset of convection, i.e., only thermal conduction, the heat transport is found to depend strongly on the layer ratio. The interface between the two layers can be broken up for certain conditions [43].

In this paper, we investigate the flow coupling of the large-scale circulations in two-layer turbulent thermal convection. We first revisit the experimental findings in Ref. [41], concerning the flow states of two interacting LSCs and their stochastic properties of cessations and reversals. Motivated by the intriguing experimental phenomena, we formulate a physically based, low-dimensional model consisting of two sets of stochastic differential equations to describe the diffusive behavior of the two LSCs as well as their thermal and mechanical interactions. The model can largely account for the two preferred flow states of thermal and viscous coupling, and provides new understanding of the mechanism of flow reversals, explaining the more frequent reversal events that arise in two-layer turbulent convection systems.

II. EXPERIMENTAL RESULTS

The experiment was performed using an apparatus described before [41]. We used a cylindrical container with height $H = 38.4$ cm and diameter $D = 19.0$ cm, yielding an aspect ratio $\Gamma = D/H = 0.5$. Two immiscible fluids, with a water layer overlying a Fluorinert electronic fluid (FC77) layer, are used as the working fluid. The two fluid layers both have a fluid height $H = 19.2$ cm, thus the aspect ratio of each fluid layer is unity (see the schematic drawing for the flow configuration in Fig. 1). To diagnose the flow structures of the LSCs, six groups of thermistors were installed at fluid heights $H/8$, $H/4$, $3H/8$, $5H/8$, $3H/4$, and $7H/8$ from the bottom plate, respectively. At each fluid height, eight thermistors are equally spaced azimuthally to measure the local fluid temperatures T_i , which are fitted using the function $T_i = T_0 + \delta \cos(i\pi/4 - \theta)$, $i = 1, \dots, 8$, to determine at the corresponding fluid height the thermal amplitude δ and azimuthal orientation θ of the LSCs. Hereafter, we use subscripts “ w ” and “FC” to denote quantities measured in water and FC77, respectively, and discuss here results of the LSC amplitudes δ_w , δ_{FC} and orientations θ_w , θ_{FC} measured at two fluid heights $3H/4$ and $H/4$. In the experiment a constant heat flux was applied at the bottom boundary of the FC77 layer, and the temperature of the top boundary of the water layer maintained a constant. Since the physical properties (e.g., α , κ , and ν) of the two fluid layers are different, the convective flows adjust spontaneously the temperature differences across each

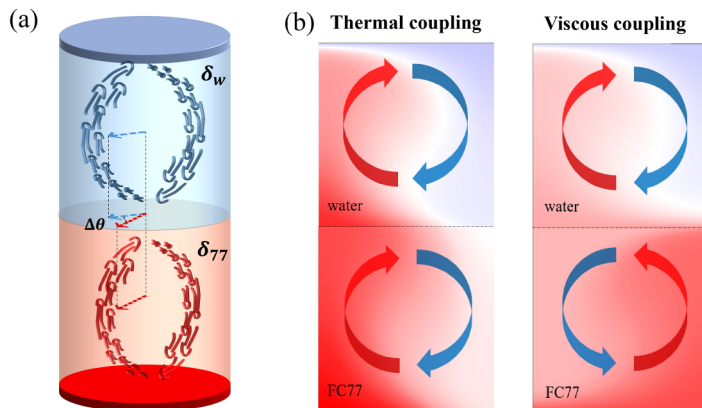


FIG. 1. (a) A schematic drawing of two-layer RB convection system that shows the main coherent structures in this system, thermal plumes and large-scale convection rolls. The evolution process of plumes illustrates the circulating direction and the red and blue dashed arrows present the azimuthal orientation θ of LSC roll of FC77 and water, respectively. (b) Schematic of the flow configurations in the flow modes of thermal coupling (left) and viscous coupling (right). The upwelling (downwelling) flow of each LSC roll is shown by the red (blue) arrow. The background color represents conceptually variation of the fluid temperature.

fluid layers. The bulk temperature of the water and FC77 layer were found to be 15°C and 37°C , respectively. We thus determine the control parameters of convection for each layer $\text{Pr}_w = 8.1$, $\text{Pr}_{\text{FC}} = 19.6$, and $\text{Ra}_w = 1.23 \times 10^9$, $\text{Ra}_{\text{FC}} = 1.59 \times 10^{11}$.

Figures 2(a) and 2(b) present experimentally measured time series of the LSC temperature amplitudes $\delta/\langle\delta\rangle$ in the FC77 and water layers, respectively. We see that the flow strengths of the two LSC rolls exhibit markedly different dynamical features: while δ_w maintains relatively constant near its mean value and never drops below the critical value of cessation during the whole experimental time, δ_{FC} fluctuates more intensively with frequent cessations. Here we adopt the criterion $\delta \leq 0.25\langle\delta\rangle$ to identify cessation events [15] as indicated by the horizontal dashed lines.

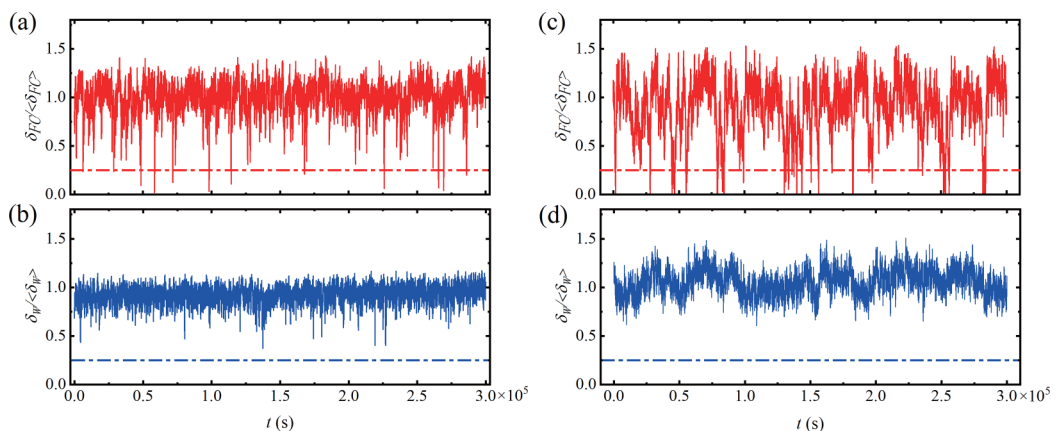


FIG. 2. Time series of the normalized temperature amplitude $\delta/\langle\delta\rangle$ for the LSCs in the FC77 fluid layer (a), (c) and in the water layer (b), (d). Results for $\text{Ra}_{\text{FC}} = 1.59 \times 10^{11}$ and $\text{Ra}_w = 1.23 \times 10^9$. Experimental data (a), (b) are compared with the model data (c), (d). The dash-dotted lines denote the threshold value $\delta_c = 0.25\langle\delta\rangle$ used to define cessations.

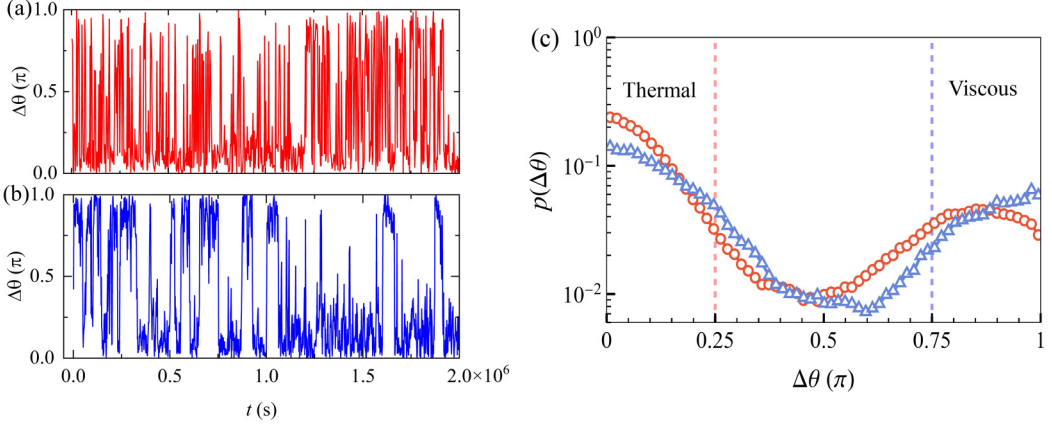


FIG. 3. Experimental (a) and modeling (b) results of the time series $\Delta\theta(t)$ that represents the flow states of the two LSCs. (c) PDFs of $\Delta\theta$ calculated using the experimental data (red circles) and model results (blue triangles). The two vertical dashed lines at $\Delta\theta = \pi/4$ and $3\pi/4$ are used as reference lines to define the flow states of thermal and viscous coupling.

To describe the relative azimuthal orientation of the two LSC rolls, we introduce the azimuthal angular difference $\Delta\theta = |\theta_{\text{FC}} - \theta_w|$ as a flow state parameter to analyze their coupling dynamics. As illustrated in Fig. 1(b), the flow state of $\Delta\theta = 0$, i.e., the upgoing (or downgoing) thermal plumes of the LSCs are positioned at the same side of the container, is defined as a flow state of thermal coupling. In the flow state of viscous coupling ($\Delta\theta = \pi$), thermal plumes of the two rolls move in same direction at the interface of the two layers. $\Delta\theta$ is reduced to $[0, \pi]$ in our analysis because of the azimuthal symmetry of the flow coupling dynamics in our cylindrical cell. Figure 3(a) shows a long time series of $\Delta\theta(t)$ acquired experimentally over a period of 25 days. In addition to its stochastic fluctuations covering the full azimuthal range, there exist apparently two preferred relative azimuthal orientations between the two LSC planes, i.e., $\Delta\theta = 0$ and π . Figure 3(c) presents the probability density function (PDF) of $\Delta\theta$. One sees that $p(\Delta\theta)$ has a maximum close to 0 and a second peak near π , corresponding to the flow states of thermal and viscous coupling, respectively.

To gain more insights into the preferred orientations of the two LSCs, we present in Figs. 4(a) and 4(b) the joint PDFs of δ and $\Delta\theta$ for the convection rolls in the FC77 layer and the water layer, respectively. It is seen that two prominent peaks of the PDFs locate at $\Delta\theta \approx 0$ and π for both rolls when $\delta \approx \langle \delta \rangle$.

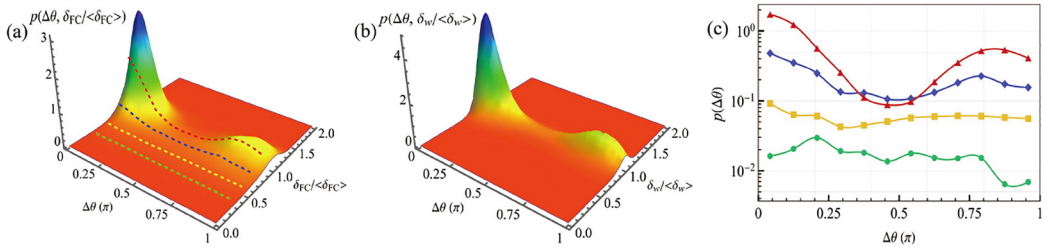


FIG. 4. Experimental results of the joint PDF $p(\Delta\theta, \delta/\langle\delta\rangle)$ for the LSC in the FC77 layer (a) and in the water layer (b). (c) Results of $p(\Delta\theta)$ for given values of $\delta_{\text{FC}}/\langle\delta_{\text{FC}}\rangle$. Green circles: $0.34 \leq \delta_{\text{FC}}/\langle\delta_{\text{FC}}\rangle \leq 0.36$, yellow squares: $0.54 \leq \delta_{\text{FC}}/\langle\delta_{\text{FC}}\rangle \leq 0.56$, blue diamonds: $0.74 \leq \delta_{\text{FC}}/\langle\delta_{\text{FC}}\rangle \leq 0.76$, red triangles: $0.94 \leq \delta_{\text{FC}}/\langle\delta_{\text{FC}}\rangle \leq 0.96$. These profiles are represented by the four dashed lines in panel (a) correspondingly.

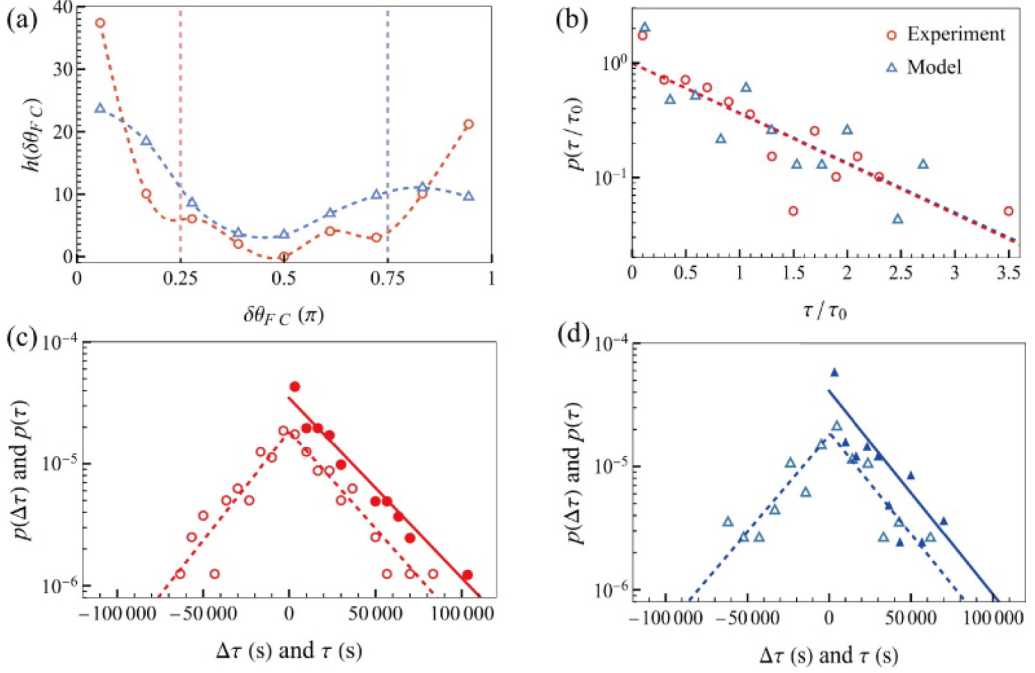


FIG. 5. (a) The histogram $h(\delta\theta_{FC})$ of orientation change of the FC77 roll during cessation events. Red circles: experimental data. Blue triangles: model results. (b) The PDF of the time interval τ between two successive cessation events $p(\tau/\tau_0)$. The red (blue) dashed line represents the fitted exponential function $p(\tau/\tau_0) = \exp(-\tau/\tau_0)$ with $\tau_0 = 2.94 \times 10^4 s$ ($2.72 \times 10^4 s$) for the experimental (modeling) data. (c), (d) Experimental and modeling results of $p(\tau)$ (filled symbols) and $p(\Delta\tau)$ (open symbol). The dashed (solid) lines indicate the fitted exponential distributions. See text for discussions.

With decreasing flow strength we see that the height of both peaks of $p(\Delta\theta, \delta_{FC}/\langle\delta_{FC}\rangle)$ for the FC77 roll decreases gradually. $p(\Delta\theta, \delta_{FC}/\langle\delta_{FC}\rangle)$ becomes relatively flattened for small δ_{FC} . The δ -dependence of $p(\Delta\theta)$ for the FC77 roll can be seen more clearly in a semilog plot in Fig. 4(c), which shows $p(\Delta\theta)$ for various ranges of flow strength δ_{FC} . One sees that the two maxima of $p(\Delta\theta)$ are evident near $\Delta\theta \approx 0$ and π in the range of $0.75 \leq \delta_{FC}/\langle\delta_{FC}\rangle \leq 0.95$. When δ_{FC} decreases the peak-structure weakens and disappears for $\delta_{FC} \approx 0.55\langle\delta_{FC}\rangle$ and $p(\Delta\theta)$ becomes nearly independent of $\Delta\theta$. For even lower value of flow strength $\delta_{FC} = 0.35\langle\delta_{FC}\rangle$, interestingly, we note that $p(\Delta\theta)$ appears minimum near $\Delta\theta = \pi$, and there is overall a tendency that the ratio of $p(\Delta\theta = \pi/2)/p(\Delta\theta = 0, \pi)$ increases with decreasing δ_{FC} . The joint PDF of the water roll decreases sharply with decreasing δ_w and presents no clear dependence on $\Delta\theta$ as shown in Fig. 4(b). These results indicate that with small flow strength the two LSC rolls have a significant probability to align perpendicularly ($\Delta\theta = \pi/2$), and that flow cessations in the FC77 fluid layer may be achieved through a new dynamical process of flow coupling.

As the FC77 roll experiences cessation frequently, we examine the histogram $h(\delta\theta_{FC})$ of its orientation change over a cessation event. Here the orientation change for cessation is computed for the whole cessation event which begins when δ_{FC} departs from its most probable value, reaching a lowest value below the critical value $0.25\langle\delta_{FC}\rangle$ for cessation. A cessation event ends when the LSC strength resumes and δ_{FC} returns to its most probable value. Figure 5(a) shows that $h(\delta\theta_{FC})$ of the FC77 roll exhibits two prominent maxima at $\Delta\theta = 0$ and π . The first maximum for $\Delta\theta = 0$ suggests that after cessation events the LSC plane in the FC77 layer often returns to its original azimuthal orientation. The second maximum at $\Delta\theta = \pi$ indicates, however, that

there is a significant probability that the FC77 roll experiences reversals in flow direction during cessation events. We stress that the measured occurrence frequency of flow reversals in the FC77 layer $\omega = 1.3 \text{ day}^{-1}$ is over one order of magnitude greater than that for single-layer convection with similar Ra and Pr [44].

III. MODEL RESULTS

A. Derivation of the model

In this section we introduce our theoretical model that describes the dynamics of two neighboring, vertically aligned LSCs in two-layer turbulent convection. We first revisit the previously derived model by Brown and Ahlers [18,19], devoted to describe the behavior of a single-roll LSC. Motivated by the NS equations, this model consists of a pair of stochastic differential equations that represent in large timescale the deterministic motion of the LSC structure, and in short timescale the stochastic fluctuations owing to the background turbulence. The flow strength of the LSC can be described by the fluid velocity on the circulating plane u_ϕ . For this degree of freedom, only the buoyancy and viscous drag terms contribute to the acceleration of u_ϕ . Therefore, the NS equation of fluid motion over the vertical plane can be written as

$$\dot{u}_\phi = \alpha g(T - T_0) + \nu \nabla^2 u_\phi. \quad (1)$$

Experimental measurements [15,28,44,45] have shown that the azimuthal temperature profile $T(\theta)$ of a single-roll LSC can be interpolated as: $T(\theta) = T_0 + \delta \cos(\theta_0 - \theta)$, where T_0 is mean temperature of working fluid over a horizontal plane and δ is the temperature amplitude which is found to be proportional to the flow strength of the LSC [19]. For a two-layer convection system, the interaction of two vertically aligned LSC rolls influences the temperature profiles for both fluid layers. We suggest that the azimuthal temperature profile over the lower fluid layer can be described as

$$T_1 = T_{10} + \delta \cos(\theta_1 - \theta) + a' \delta_2 I(\Delta\theta).$$

Here we use subscripts 1, 2 to denote quantities in the lower and upper fluid layer, respectively. Note that the temperature profile for the upper layer T_2 has a similar equation except swapping the subscripts of 1 and 2. The last term $a' \delta_2 I(\Delta\theta)$ represents the influence on T_1 owing to thermal coupling of the two LSCs, which is proportional to the temperature amplitude δ_2 of the upper LSC. a' is an attenuation coefficient to be used as a fitting parameter in the range $0 < a' < 1$. The thermal coupling factor $I(\Delta\theta)$ depends on the relative azimuthal orientation $\Delta\theta$ of the two LSC rolls.

We suggest that the azimuthal angular difference $\Delta\theta$ of two LSC rolls plays crucial roles in their thermal interaction. We consider the following states of flow coupling:

(i) When $\Delta\theta = 0$, the two LSC rolls are corotating [see the left column of Fig. 1(b)]. The hot (cold) plumes forming the two LSCs appear at the same azimuthal orientation near the sidewall and thus enhance each other their thermal amplitude. Under this condition, the buoyancy forcing on each LSC rolls is strengthened by both thermal diffusion and heat advection provoked owing to the other roll. The strength of thermal coupling between the two LSCs is maximum.

(ii) When $\Delta\theta = \pi$, the two LSC rolls are counterrotating. In this situation the hot (cold) plumes appear at the opposite side of the cell and reduce, to some extent, the azimuthal temperature anomaly on each fluid layer. However, in this flow state the two LSC flows are in the same direction at the fluid interface and thus heat transports can be considerably enhanced through flow advection [see illustration in the right column of Fig. 1(b)]. Therefore the LSC flow in each fluid layer can still be strengthened.

(iii) When $\Delta\theta = \pi/2$ or $3\pi/2$, the circulating planes of the two LSCs are orthogonal to each other. The interacting strength of the two LSCs in this flow state is minimum.

According to these analyses, we suggest that the thermal coupling factor consists two terms $I(\Delta\theta) = \bar{I} + \tilde{I}(\Delta\theta)$, where the $\Delta\theta$ -independent term \bar{I} represents the reduced (increased) mean temperature of the lower (upper) layer owing to the overall enhanced heat transport by the upper

(lower) LSC flow. $\tilde{I}(\Delta\theta)$ is an alternating component of $I(\Delta\theta)$ fulfilling $\int_0^{2\pi} \tilde{I}(\Delta\theta) d\Delta\theta = 0$, which is hypothesized to be a function of $\Delta\theta$ as follows:

$$\tilde{I}(\Delta\theta) = (I_0 - 1) \cos(2\Delta\theta) + (2 - I_0) \cos(\Delta\theta).$$

Here I_0 denotes the value of $I(\Delta\theta)$ for $\Delta\theta = 0$, and $I_0 = \bar{I} + 1$. We assume this functional form of thermal coupling as the simplest way to account for its periodicity of $\Delta\theta$. $\tilde{I}(\Delta\theta)$ has a local maximal value when the two LSCs are either in the corotating state ($\Delta\theta = 0$), or in the counterrotating state ($\Delta\theta = \pi$). Furthermore, we expect that $0 < \tilde{I}(\pi)/\tilde{I}(0) < 1$ as thermal coupling of two corotating LSCs is even stronger. Since $\tilde{I}(\pi)/\tilde{I}(0) = 2I_0 - 1$, we constrain the parameter range of I_0 in our model as $3/2 < I_0 < 2$. Last, $\tilde{I}(\Delta\theta)$ reaches a local minimum when the two LSC planes are orthogonal to each other ($\Delta\theta = \pi/2$ or $3\pi/2$).

With the expression of $\tilde{I}(\Delta\theta)$ one can obtain the functional form of the azimuthal temperature profile in two-layer convection:

$$T_1 = \bar{T}_1 + \delta_1 \cos(\theta_1 - \theta) + a' \delta_2 \tilde{I}(\Delta\theta).$$

Here $\bar{T}_1 = T_{10} + \delta_2 \bar{I}$ denotes the mean fluid temperature which is independent of the azimuthal coordinate. a' is the thermal coupling coefficient. In RB convection the flow strength of the LSC fluctuates in a shorter timescale compared to the orientational change of the LSC plane. Thus we decompose the thermal amplitude δ_2 into a mean value δ_{20} and a fluctuating term δ_2 , i.e., $\delta_2 = \delta_{20} + \delta_2$. When evaluating the mean fluid temperature of the upper layer in a relatively large timescale, we approximate that $\delta_2 \approx \delta_{20}$ and obtain $\bar{T}_1 = T_{10} + \delta_{20} \bar{I}$.

Now we calculate the buoyancy force on the LSC roll in the lower fluid layer according to Eq. (1). Using a step function $S(\theta - \theta_1) = 1$ (-1) when $|\theta - \theta_1|$ is smaller (larger) than $\pi/2$ to present the direction of buoyancy, we take the volume average of the lower fluid layer $\langle \alpha_1 g(T_1 - \bar{T}_1) \rangle_V = 1/(2V) \int \alpha_1 g(T_1 - \bar{T}_1) dV = 1/(2\pi) \int_0^{2\pi} \alpha_1 g(T_1 - \bar{T}_1) S(\theta - \theta_1) d\theta$, and use the expression of T_1 to obtain

$$\langle \alpha_1 g(T_1 - \bar{T}_1) \rangle_V = \frac{2g\alpha_1\delta_1}{3\pi} + a \frac{2g\alpha_1\delta_2}{3\pi} \tilde{I}(\Delta\theta),$$

where $a = \pi a'/2$. We see that offset term \bar{T}_1 which presents the increased (decreased) mean fluid temperature due to the LSC flow coupling, has no contribution to the buoyancy force on the LSC rolls.

The viscous force term in Eq. (1) originates from drag force that occurs with the viscous boundary layers (BLs). In two-layer convection, the drag force applied on the LSC rolls consists of the wall drag near the nonslip boundaries of the sidewall and plates, and the flow-coupling drag at the fluid-fluid interface owing to the different flow velocities of the two LSC rolls. In computing the wall drag for the LSC in the lower layer, we assume a linear velocity profile within the viscous BLs and a Prandtl-Blasius form of the BL thickness $\lambda = H/(2\sqrt{\text{Re}})$ [46,47] with Reynolds number $\text{Re} \equiv HU/\nu$ and the LSC flow speed U . The viscous BLs near the bottom plate and the lower half of the sidewall thus occupy a volume fraction of the lower fluid layer equal to $5\lambda_1/H$ (see, e.g., Ref. [19]), with λ_1 being the viscous boundary layer thickness in the FC77 layer. We obtain the volume-average of the wall drag, $\langle \nu_1 \nabla^2 u_{1\phi}^w \rangle_V \approx \langle -\nu_1 U_1 / \lambda_1^2 \rangle_V = -10\nu_1^{1/2} U_1^{3/2} / H^{3/2}$, where U_1 is the mean flow velocity of the LSC in the FC77 layer. The magnitude of the viscous drag at the fluid interface is determined by the fluid velocity difference $U_1 - U_0$. Here U_0 is fluid velocity of the upper layer near the interface, which is assumed to be a projection of the upper roll velocity U_2 along the direction of the lower roll, i.e., $U_0 = -b \cos(\Delta\theta) U_2$. And b is an coefficient for viscous coupling to be used as a fitting parameter in the range $0 < b < 1$. The viscous BLs near the fluid-fluid interface has a volume fraction λ_1/H of the lower fluid layer, thus we can derive the volume-average of the viscous drag at the fluid interface $\langle \nu_1 \nabla^2 u_{1\phi}^i \rangle_V \approx \langle \nu_1 [-b \cos(\Delta\theta) U_2 - U_1] / \lambda_1^2 \rangle_V =$

$-2[b \cos(\Delta\theta)U_2 + U_1]v_1^{1/2}U_1^{1/2}/H^{3/2}$. Combining these two types of viscous force yields

$$\langle v_1 \nabla^2 u_{1\phi} \rangle_V = -\frac{12v_1^{1/2}U_1^{3/2}}{H^{3/2}} - b\frac{2v_1^{1/2}U_1^{1/2}U_2}{H^{3/2}} \cos(\Delta\theta).$$

We have assumed that the strength of viscous coupling of two LSC rolls is a cosine function of their orientational difference $\Delta\theta$, accounting for its periodicity of 2π and the facts that the two LSC rolls reinforce (attenuate) each other when $|\Delta\theta|$ is less (larger) than $\pi/2$. Such a coupling effect is maximum when the two rolls are lined up onto the same plane with $\Delta\theta = 0$ or π , but becomes zero when the two rolls are orthogonal to each other with $\Delta\theta = \pi/2$ or $3\pi/2$. Note that if $U_2 = 0$ the expression of the viscous force is degenerated into that for single-roll LSC [19].

Since the bulk velocity profile $u_\phi \approx 2rU/H$ varies approximately linearly with r [48,49], we obtain the volume-averaged fluid acceleration $\langle \dot{u}_\phi \rangle_V = 2\dot{U}/3$. Based on Eq. (1), the equation of motion for the LSC velocity in the lower fluid layer can be represented as

$$\frac{2\dot{U}_1}{3} = \frac{2g\alpha_1\delta_1}{3\pi} + a\frac{2g\alpha_1\delta_2}{3\pi}\tilde{I}(\Delta\theta) - \frac{12v_1^{1/2}U_1^{3/2}}{H^{3/2}} - b\frac{2v_1^{1/2}U_1^{1/2}U_2}{H^{3/2}} \cos(\Delta\theta). \quad (2)$$

Both the flow velocity U and temperature δ are measures of the LSC strength. They are found to be instantaneously proportional to each other, with their proportionality constant satisfying $2g\alpha_1\delta_1/(3\pi) = 12v_1U_1\text{Re}^{1/2}/H^2$ [19]. We thus substitute U_1 with δ_1 to simplify the equation which then contains only variables of temperature amplitudes δ_1 and δ_2 that can be measured in the experiments. Switching the subscripts of 1 and 2, the equations for the flow strength of two vertically aligned LSCs can be rearranged as two Langevin equations with the stochastic term $f_\delta(t)$ representing the random force owing to the background small-scale turbulent fluctuations:

$$\dot{\delta}_1 = \frac{\delta_1}{\tau_{\delta_1}} - \frac{\delta_1^{3/2}}{\delta_{10}^{1/2}\tau_{\delta_1}} + a\frac{\delta_2}{\tau_{\delta_1}}\tilde{I}(\Delta\theta) - b\frac{v_2\text{Re}_2}{v_1\text{Re}_1}\frac{\delta_1^{1/2}\delta_2}{6\delta_{20}\tau_{\delta_1}} \cos(\Delta\theta) + f_{\delta_1}(t), \quad (3)$$

$$\dot{\delta}_2 = \frac{\delta_2}{\tau_{\delta_2}} - \frac{\delta_2^{3/2}}{\delta_{20}^{1/2}\tau_{\delta_2}} + a\frac{\delta_1}{\tau_{\delta_2}}\tilde{I}(\Delta\theta) - b\frac{v_1\text{Re}_1}{v_2\text{Re}_2}\frac{\delta_2^{1/2}\delta_1}{6\delta_{10}\tau_{\delta_2}} \cos(\Delta\theta) + f_{\delta_2}(t). \quad (4)$$

Here we have defined the mean LSC amplitude $\delta_0 \equiv 18\pi\Delta T\sigma\text{Re}^{3/2}/\text{Ra}$ and the timescale $\tau_\delta \equiv H^2/18v\text{Re}^{1/2}$. The stochastic term f_δ is modeled by Gaussian noise, which has a zero mean and an autocorrelation $\langle f_\delta(t_1)f_\delta(t_2) \rangle_t = 2(D_\delta/\tau_\delta^2)\delta(t_1 - t_2)$. Here $\delta(t)$ is a Dirac δ function. D_δ is the diffusion coefficient of the LSC amplitude. We note that the third and fourth terms in Eqs. (3) and (4) represent the thermal and viscous coupling effect of two vertically aligned LSCs, respectively. Their competition may lead to an increased or decreased growth rate of the flow strength δ for each LSC roll, as we will discuss in detail in following sections.

To describe the azimuthal motion of the LSC planes, we consider the azimuthal component of the NS equation

$$\dot{u}_\theta + \vec{u} \cdot \vec{\nabla} u_\theta = \nu \nabla^2 u_\theta. \quad (5)$$

Here the advection term presents mainly the rotational inertia of the LSC which provides a variable damping force for the azimuthal motion of the LSC planes. Since the viscous drags across the BLs near the rigid walls and the fluid interface are small compared to this damping term [18,19], they are neglected in the present model. Since $\dot{u}_\theta = H\dot{\theta}$, and only the component corresponding to the rotational inertia of the LSC in the vertical plane is significant for the advection term $\vec{u} \cdot \vec{\nabla} u_\theta \approx \partial u_\theta / \partial \phi (u_\phi / r) \sim U\dot{\theta}$, we take volume averages of these terms to obtain: $H\dot{\theta}/3 + 2U\dot{\theta}/3 = 0$. Introducing a second stochastic term $f_\theta(t)$ to represent the random forcing on $\dot{\theta}$ owing to the turbulent background fluctuations, and converting U to δ using their proportional relation, we arrive at the second sets of Langevin equations for the azimuthal rotation of the two

TABLE I. The values of the main input parameters in model.

| a | b | I_0 | $\delta_{\text{FC},0}$ (K) | $\delta_{w,0}$ (K) | $D_{\delta_{\text{FC}}}$ (K^2/s) | D_{δ_w} (K^2/s) | $D_{\dot{\theta}_{\text{FC}}}$ (rad^2/s^3) | $D_{\dot{\theta}_w}$ (rad^2/s^3) |
|------|------|-------|----------------------------|--------------------|--|--|--|--|
| 0.13 | 0.22 | 1.76 | 0.21 | 0.57 | 0.92×10^{-5} | 3.2×10^{-5} | 0.95×10^{-4} | 1.1×10^{-5} |

LSC rolls:

$$\ddot{\theta}_1 = -\frac{\dot{\theta}_1 \delta_1}{\tau_{\dot{\theta}_1} \delta_{10}} + f_{\dot{\theta}_1}(t), \quad (6)$$

$$\ddot{\theta}_2 = -\frac{\dot{\theta}_2 \delta_2}{\tau_{\dot{\theta}_2} \delta_{20}} + f_{\dot{\theta}_2}(t). \quad (7)$$

Here $f_{\dot{\theta}}$ is modeled as Gaussian noise which is independent of f_{δ} , $\langle f_{\dot{\theta}}(t_1) f_{\dot{\theta}}(t_2) \rangle_t = 2(D_{\dot{\theta}}/\tau_{\dot{\theta}}^2)\delta(t_1-t_2)$. $\tau_{\dot{\theta}} \equiv H^2/2\nu\text{Re}$ defines the timescale for the azimuthal dynamics of the LSCs and $D_{\dot{\theta}}$ is the diffusivity coefficient of $\dot{\theta}$.

Equations (3), (4), (6), and (7) compose the model for the dynamics of two coupling LSCs. They are four stochastic ordinary differential equations (ODEs) with variables ($\delta_1, \delta_2, \dot{\theta}_1, \dot{\theta}_2$) presenting the strengths and the azimuthally rotating rate of the two LSC rolls. The coefficients of the model including the mean temperature amplitude δ_0 , and the timescales τ_{δ} and $\tau_{\dot{\theta}}$, and the diffusion constants D_{δ} and $D_{\dot{\theta}}$ represent the dynamical properties of one LSC roll and are determined experimentally. Our model contains three unknown parameters (a, b and I_0) which reveal the degree of flow coupling of the two LSCs. Using our experimental data of $p(\Delta\theta, \delta/\langle\delta\rangle)$ for the flow coupling states, we give details of the methods to constrain and optimize their values in the Appendix. A list of the model parameter values are given in Table I.

B. Model results

Figures 2(c) and 2(d) show the calculated time series of normalized flow strength $\delta/\langle\delta\rangle$ for the two LSC rolls, capturing the main feature of the experimental results. The time trace $\delta/\langle\delta\rangle$ for each LSC exhibits similarities to the single-roll case observed in experiments, for example, the amplitude of the LSC appears stable around their mean value but with occasional drastic fluctuations. Moreover, our model shows that the frequency of cessation differs markedly for the two LSCs. Using $\delta_c = 0.25\delta_0$ as the threshold for cessation events, our model predicts that flow cessation occurs very frequently in the FC77 layer [Fig. 2(c)], with an occurrence frequency of $\omega_{\text{FC}} = 4.88 \text{ day}^{-1}$ that is even twice higher than that in single-roll case [41,44]. However, no flow cessation is observed in the water layer in a timescale of 23 days [Fig. 2(d)]. These modeling results are in good accord with the experiment.

Figure 3(b) presents model results of the azimuthal angular difference $\Delta\theta(t)$ of the two LSC rolls. Our model reproduces the large-amplitude fluctuations of $\Delta\theta$ in time, and the two preferred relative orientations of the two LSCs ($\Delta\theta = 0$ and π) as observed experimentally. These two preferred relative orientations, as previously interpreted, corresponds to the flow states of thermal and viscous couplings, respectively. Using these computational data we computer the PDF of $\Delta\theta$ for the two LSCs, and compared with the experimental data in Fig. 3(c). Our model predicts that ($\Delta\theta$) has an oscillatory profile with two prominent peaks located at $\Delta\theta = 0$ and π , and a local minimum for $\Delta\theta = \pi/2$. The close agreement between the model and experimental results indicates that the model captures the essential ingredients of flow coupling responsible for the preferred flows states observed in the experiment.

The joint PDF of δ and $\Delta\theta$ obtained from the model are illustrated in Figs. 6(a) and 6(b) for convection rolls in the FC77 and water layer, respectively. The well-marked global peaks are found around $\Delta\theta = 0$ and π with $\delta \approx \delta_0$ for both LSC rolls. With decreasing δ , the profile of $p(\Delta\theta, \delta/\langle\delta\rangle)$

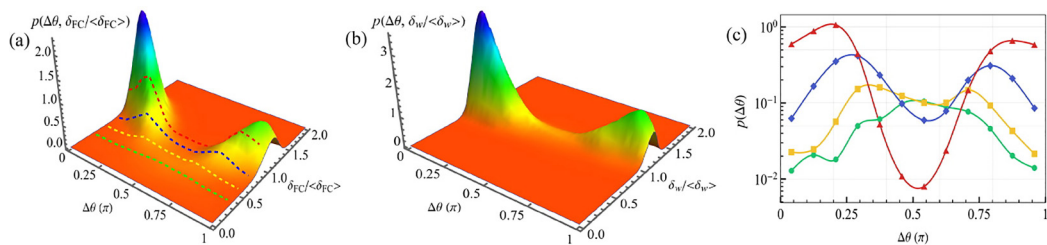


FIG. 6. Modeling results of the joint PDF $p(\Delta\theta, \delta/\langle\delta\rangle)$ for the LSC in the FC77 layer (a) and in the water layer (b). (c) Results of $p(\Delta\theta)$ for given values of $\delta_{FC}/\langle\delta_{FC}\rangle$. Green circles: $0.34 \leq \delta_{FC}/\langle\delta_{FC}\rangle \leq 0.36$, yellow squares: $0.54 \leq \delta_{FC}/\langle\delta_{FC}\rangle \leq 0.56$, blue diamonds: $0.74 \leq \delta_{FC}/\langle\delta_{FC}\rangle \leq 0.76$, red triangles: $0.94 \leq \delta_{FC}/\langle\delta_{FC}\rangle \leq 0.96$. These profiles are shown as well by four dashed lines in panel (a) correspondingly.

for the LSC roll in FC77 evolves. The magnitude of the two maxima decreases with their positions moving towards $\Delta\theta = \pi/2$. This is in stark contrast to that of the LSC roll in water for which the PDF decreases sharply towards zero irrespective of $\Delta\theta$. In Fig. 6(c) we show four profiles of $p(\Delta\theta)$ for the FC77 roll with given flow strength $\delta = (0.95, 0.75, 0.55, 0.35)\delta_0$, respectively. We see clearly the trend that the maxima of $p(\Delta\theta)$ switches from $\Delta\theta = 0, \pi$ at large δ , to $\Delta\theta = \pi/2$ when δ is small. For very low flow strength $\delta \leq 0.35\delta_0$ where flow cessation and reversal may occur, we find that the maximum of $p(\Delta\theta)$ is suited at $\Delta\theta = \pi/2$. These modeling results show, to some extent, similar features of the δ -dependence for $p(\Delta\theta)$ observed experimentally [Fig. 4(c)]. They suggest that in the present two-layer convection system, cessation and reversal events occur frequently when the two LSC rolls are in a configuration that their circulation planes are orthogonal to each other with $\Delta\theta = \pi/2$.

We examine the statistical properties of flow cessation and reversal predicted in the model. Figure 5(a) presents a histogram of the orientation change for the FC77 roll during a cessation event. We see that data curves of $h(\delta\theta_{FC})$ for both the model and experiment collapse approximately onto each other. The two maxima of $h(\delta\theta_{FC})$ suggest that after a cessation event the FC77 roll is likely to resume at its initial azimuthal orientation ($\delta\theta_{FC} = 0$), or undergoes flow reversal ($\delta\theta_{FC} = \pi$). Moreover, the data also indicate that flow reversal occurs very frequently and has a significant contribution to the stochastic behavior of the LSC in the FC77 layer. We find an occurrence frequency $\omega_{FC} = 0.97 \text{ day}^{-1}$ for flow reversal in our model, which is in reasonable agreement with the experimental observation.

To further explore the stochastic features of flow cessations in the FC77 layer, we present in Fig. 5(b) the PDF of the time interval between two successive cessation events $p(\tau/\tau_0)$. Here the exact time of a cessation is defined as the moment when the LSC strength δ_{FC} is minimum. τ is defined as the time interval between the exact times of two successive cessations. Both the experimental and modeling data are in agreement with the exponential function $p(\tau/\tau_0) = \exp(-\tau/\tau_0)$, as indicated by the fitted dashed lines. The slope of the dashed lines gives a characteristic timescale for cessation interval, $\tau_0 = 2.72 \times 10^4$ in the model, which is quite similar to the measured value $\tau_0 = 2.94 \times 10^4$.

The exponential PDF of τ indicates that the sequence of flow cessation is a Poisson processes. To substantiate this claim, we calculate the PDF of the increments between successive time intervals $\Delta\tau = \tau_{i+1} - \tau_i$. Here τ_i is the i th time interval of cessation. Figures 5(c) and 5(d) present the experimental and modeling results of $p(\Delta\tau)$ (filled symbols), respectively, which are compared with the data of $p(\tau)$ (filled symbols). While data of $p(\tau)$ are well described by $p(\tau) = c_0 \exp(-\tau/\tau_0)$ with the pre-factor $c_0 = 2.04 \times 10^{-5}$ (1.84×10^{-5}) for the experimental (modeling) results, we see that both the experimental and modeling results of $p(\Delta\tau)$ are in good agreement with the exponential distribution $p(\Delta\tau) = 0.5c_0 \exp(-\Delta\tau/\tau_0)$, with the characteristic time τ_0 determined previously. The Poissonian distributions of both τ and $\Delta\tau$ for cessation events, as seen in the

experimental and modeling data, suggest that flow cessations occur as a stochastic process and the occurrence of a cessation event is independent of each other.

IV. DISCUSSION

One of the most intriguing flow dynamics observed in the present two-layered convection system is the significantly enhanced rate of flow cessations and reversals in the FC77 layer, differing markedly from the LSC dynamics in single-layer convection. To reveal its underlying mechanism, we analyze the equation of motion for the flow strength δ of the two LSCs. Neglecting the stochastic terms in Eq. (3), and substituting δ_2 in the thermal and viscous coupling terms by its mean δ_{20} , we obtain the deterministic equation for δ_1 ,

$$\dot{\delta}_1^d = \frac{\delta_1}{\tau_{\delta_1}} - \frac{\delta_1^{3/2}}{\delta_{10}^{1/2} \tau_{\delta_1}} + a \frac{\delta_{20}}{\tau_{\delta_1}} \tilde{I}(\Delta\theta) - b \frac{\nu_2 \text{Re}_2}{\nu_1 \text{Re}_1} \frac{\delta_{10}^{1/2} \delta_1^{1/2}}{6\tau_{\delta_1}} \cos(\Delta\theta). \quad (8)$$

Similarly, the deterministic equation for δ_2 reads

$$\dot{\delta}_2^d = \frac{\delta_2}{\tau_{\delta_2}} - \frac{\delta_2^{3/2}}{\delta_{20}^{1/2} \tau_{\delta_2}} + a \frac{\delta_{10}}{\tau_{\delta_2}} \tilde{I}(\Delta\theta) - b \frac{\nu_1 \text{Re}_1}{\nu_2 \text{Re}_2} \frac{\delta_{20}^{1/2} \delta_2^{1/2}}{6\tau_{\delta_2}} \cos(\Delta\theta). \quad (9)$$

Equations (8) and (9) reduce to the deterministic amplitude equation for the LSC in a single-roll configuration if the two coupling terms are ignored [19],

$$\dot{\delta}_s^d = \frac{\delta_s}{\tau_\delta} - \frac{\delta_s^{3/2}}{\delta_0^{1/2} \tau_\delta}. \quad (10)$$

Setting $\dot{\delta}_s^d = 0$, one sees that the amplitude equation (10) has two fixed points. An unstable fixed point locates at $\delta_1^* = 0$ since $\partial \dot{\delta}_s^d(\delta)/\partial \delta_s|_{\delta=0} > 0$. There is a second fixed point at $\delta_2^* = \delta_0$ that is stable to small perturbations for δ_s because $\partial \dot{\delta}_s^d(\delta)/\partial \delta_s|_{\delta=\delta_0} < 0$. As pointed out in the pioneering work [19], the stochastic behavior of LSC cessation can be interpreted in terms of diffusion in a potential well defined by Eq. (10), $V(\delta_s) = -\int \dot{\delta}_s^d(\delta_s) d\delta = -\delta_s^2/(2\tau_\delta) + 2\delta_s^{5/2}/(5\tau_\delta \delta_0^{1/2})$. Flow cessation occurs when the LSC amplitude δ_s drops to zero owing to the random forcing from the background turbulent fluctuations, i.e., when the fluctuations of δ_s exceed the potential barrier $\Delta V \equiv V(0) - V(\delta_0) = \delta_0^2/(10\tau_\delta)$. Given by the intensity of the stochastic force f_δ one can evaluate the first-passage time for δ to escape the potential well and thus the cessation frequency $\omega = \exp(-2\Delta V_\delta/D_\delta)/(2\pi\tau_\delta)$. Using the known coefficients (i.e., δ_0 , τ_δ and D_δ) for the two LSCs, one finds that the cessation frequency of the LSC in the FC77 and the water layer are $\omega_{\text{FC}} = 0.39 \text{ day}^{-1}$ and $\omega_w = 6.7 \times 10^{-9} \text{ day}^{-1}$, respectively. Obviously one underestimates the cessation frequency of the FC77 roll in the present two-layer convection system based on the aforementioned single-roll LSC model.

We now consider the phase portrait for two coupling LSCs according to our model. Figures 7(b) and 7(c) present $\dot{\delta}_{\text{FC}}^d$ and $\dot{\delta}_w^d$ as functions of $\Delta\theta$ and $\delta/\langle\delta\rangle$ based on Eqs. (8) and (9), respectively. For comparison we show in Fig. 7(a) results of $\dot{\delta}_s^d$ in the phase space $(\delta/\langle\delta\rangle, \Delta\theta)$ for the case of single-roll LSC based on Eq. (10), whereby there exists no $\Delta\theta$ -dependence of $\dot{\delta}_s^d$ by definition. For two interacting LSCs, however, their thermal and viscous coupling effects result in new $\Delta\theta$ -depending terms in their $\dot{\delta}$ equations. The thermal coupling effect, expressed as $a\delta_{i0}\tilde{I}(\Delta\theta)/\tau_{\delta_j}$ ($i, j = 1, 2$), has positive contributions to $\dot{\delta}$ around $\Delta\theta = 0$ and π since in both states the LSC amplitudes are enhanced by heat advection. The viscous coupling effect, modeled as a drag force with its magnitude proportional to $\cos(\Delta\theta)$ [the last term in Eqs. (8) and (9)], increases δ when the two LSC rolls are counterrotating ($\Delta\theta = \pi$), but reduces δ if the two LSC rolls are corotating ($\Delta\theta = 0$). Thus the competition between the thermal and viscous coupling effects of the two LSCs determines the oscillation amplitude of $\dot{\delta}^d$ over the phase space $(\delta/\delta_0, \Delta\theta)$. In the flow state when the two LSC planes are orthogonal to each other ($\Delta\theta = \pi/2$), $\dot{\delta}^d$ for both LSCs is reduced, compared to $\dot{\delta}_s^d$ for

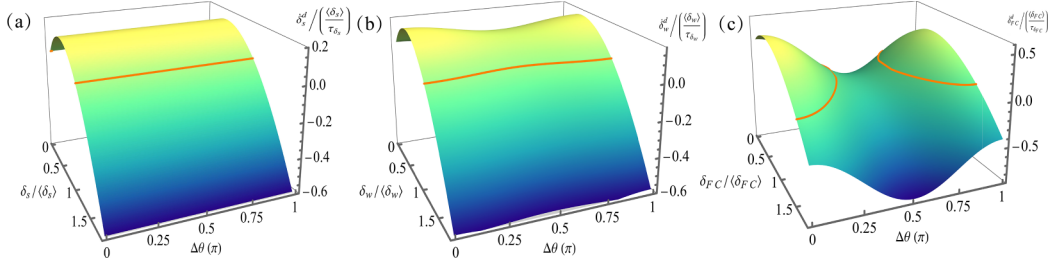


FIG. 7. The normalized time-derivative of the LSC amplitude δ^d as functions of $\Delta(\theta)$ and $\delta/\langle\delta\rangle$. Results for the LSC in a single-roll configuration (a), in the FC77 layer (b), and in the water layer (c). δ^d is calculated based on Eqs. (8)–(10). For a single-roll LSC δ_s^d is by definition independent of $\Delta(\theta)$, but shown as well in panel (a) as a three-dimensional phase surface $\delta_s^d(\Delta(\theta), \delta/\langle\delta\rangle)$ for comparisons. The orange line is the intersection lines of the surface $\delta^d(\Delta(\theta), \delta/\langle\delta\rangle)$ with the plane $\delta^d = 0$, which is the collection of stable fixed points.

a single-roll LSC. Such a reduction in δ^d is attributed to the background fluid cooling (warming) in the FC77 (water) layer which reduces the buoyancy forcing on the LSC structure, a global effect of heat advection and diffusion in the present two-layer convection system.

We evaluate the relative strength of thermal coupling effect compared to the buoyancy forcing on the two LSCs. We calculate the ratios of the third term (representing thermal coupling effect) over the first term (representing buoyancy force) in Eqs. (8) and (9). Taking time-average for the LSC amplitudes $\delta_i (i = 1, 2)$ and approximating $\tilde{T}(\Delta\theta)$ as unity, we find the ratios are $a\delta_{20}/\delta_{10} = 0.34$ and $a\delta_{10}/\delta_{20} = 0.05$ for the LSC in the FC77 and water layer, respectively. They imply that although the thermal coupling effect is insignificant in the water layer, it plays a crucial role in the amplitude equation of the FC77 roll. For this reason prominent oscillations appear on the phase surface $\delta_{FC}^d(\delta/\langle\delta\rangle, \Delta\theta)$ for the FC77 roll [Fig. 7(c)], with pronounced crests and trough arising at $(\Delta\theta = 0, \pi, 2\pi)$ and $(\Delta\theta = \pi/2)$, respectively. The phase surface of $\delta_w^d(\delta/\langle\delta\rangle, \Delta\theta)$ for the LSC roll in water, however, is relatively flat along the axis of $\Delta\theta$ [see Fig. 7(b)]. The ratios of the viscous coupling effect over the buoyancy forcing can be assessed, taking the magnitude of the fourth term in Eqs. (8) and (9), as $b\nu_2\text{Re}_2/(6\nu_1\text{Re}_1) = 0.01$ for the FC77 roll and $b\nu_1\text{Re}_1/(6\nu_2\text{Re}_2) = 0.09$ for the water roll. We see that the viscous coupling effect on either LSC rolls is insufficient to produce significant variations of the phase surface $\delta_{FC}^d(\delta/\langle\delta\rangle, \Delta\theta)$.

We seek for physical interpretations for the dissimilar effects of thermal coupling on the two LSCs and explain their different dynamics. In the experiment a constant heat flux density Q was applied through the two fluid layers. For the parameter regime of $10^9 \leq \text{Ra} \leq 10^{11}$ and $8 \leq \text{Pr} \leq 20$, the Nusselt number, which measures ratio of the effective thermal conductivity of the convecting fluid to the thermal conductivity λ of the quiescent fluid, can be described approximately as $\text{Nu} = QH/(\lambda\Delta T) \approx 0.05 \text{Ra}^{1/3}$ [50]. Substituting the definition expression for Ra, one finds that $Q \propto (\lambda^3\alpha/\kappa\nu)^{1/3}\Delta T^{4/3}$. Given by the physical properties of the two fluid layers (i.e., $\alpha_{FC} = 1.4 \times 10^{-3} \text{K}^{-1}$, $\kappa_{FC} = 3.4 \times 10^{-4} \text{cm}^2\text{s}^{-1}$, $\nu_{FC} = 6.6 \times 10^{-3} \text{cm}^2\text{s}^{-1}$, $\lambda_{FC} = 6.1 \times 10^{-4} \text{W cm}^{-1}\text{K}^{-1}$, and $\alpha_w = 1.5 \times 10^{-4} \text{K}^{-1}$, $\kappa_w = 1.4 \times 10^{-3} \text{cm}^2\text{s}^{-1}$, $\nu_w = 1.1 \times 10^{-2} \text{cm}^2\text{s}^{-1}$, $\lambda_w = 5.9 \times 10^{-3} \text{W cm}^{-1}\text{K}^{-1}$), one can evaluate the values of the combined coefficient $\lambda^3\alpha/\kappa\nu$ to be $1.34 \times 10^{-7} \text{W}^3 \text{cm}^6 \text{K}^{-4}$ and $1.88 \times 10^{-6} \text{W}^3 \text{cm}^6 \text{K}^{-4}$ for the FC77 and the water layer, respectively. We then determine the ratio of the temperature differences over the two fluid layers $\Delta T_{FC}/\Delta T_w = 1.94$, which is in good agreement with the measured value 1.93. It hints that the larger temperature difference crossing the FC77 layer is mainly attributed to its relatively lower thermal conductivity. Thus we can predict the ratio of the Rayleigh numbers for the two fluid layers $\text{Ra}_{FC}/\text{Ra}_w = 130.3$ with its experimentally determined value being 129.6. The Reynolds number for the LSC can be approximated as well in this flow regime $\text{Re} = UH/\nu \propto \text{Ra}^{4/9}\text{Pr}^{-2/3}$ [50]. We can then express the time-averaged LSC amplitude $\delta_0 \equiv 18\pi\Delta T\sigma\text{Re}^{3/2}/\text{Ra}$, as defined in the equations of motion (3) and (4), in terms of

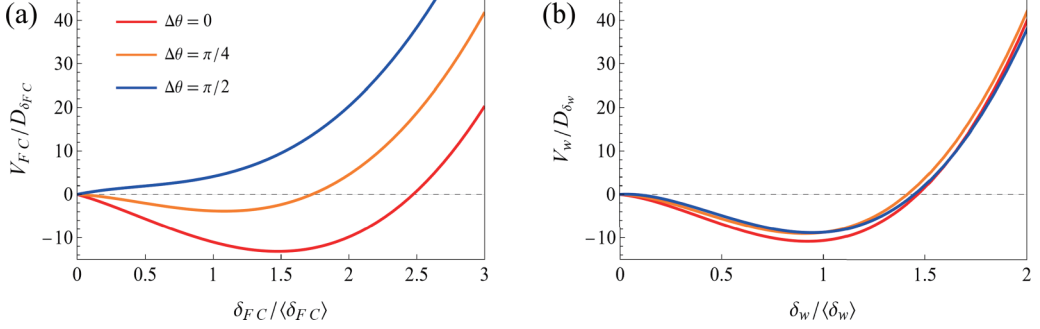


FIG. 8. The potential $V(\delta)$ for various flow states $\Delta\theta = 0$ (red line), $\Delta\theta = \pi/4$ (orange line), and $\Delta\theta = \pi/2$ (blue line). Results for the LSC in the FC77 layers (a) and in the water layer (b).

ΔT and the parameters of the fluid properties $\delta_0 \propto (\kappa \nu \alpha^{-1} \Delta T^2)^{1/3}$. We can now evaluate the ratios of the strength of thermal coupling over buoyancy forcing for the LSC in the FC77 layer, which is given by $a\delta_{w,0}/\delta_{FC,0} \propto (\kappa \nu \alpha^{-1} \Delta T^2)_w^{1/3} / (\kappa \nu \alpha^{-1} \Delta T^2)_{FC}^{1/3}$, according to Eqs. (8) and (9). Although the temperature difference ΔT_w in the water layer is smaller than in the FC77 layer, the thermal expansion coefficients of the FC77 layer is approximately one order in magnitude larger than that of water, i.e., $\alpha_{FC}/\alpha_w = 9.32$. Thus a thermal perturbation of smaller amplitude generated from the water layer, presumably produced by thermal plumes detached from the LSC therein, may result in considerably large buoyancy acceleration of the LSC in the FC77 layer. We find that this is the dominating factor that contributes to the prominent effect of thermal coupling in the FC77 layer. We conclude that it is the different physical properties of the two fluid layers that gives rise to the distinct dynamics the two LSCs in the present two-layer convection system.

In Figs. 7(a)–7(c) we show in orange curves the intersection lines of the surface $\dot{\delta}^d(\Delta\theta, \delta/\langle\delta\rangle)$ with the plane $\dot{\delta}^d = 0$. They are a collection of stable fixed points $\delta^*(\Delta\theta)$ since $\partial\dot{\delta}^d(\delta)/\partial\delta|_{\delta=\delta^*} < 0$, and if a small deviation of the LSC amplitude arises from δ^* , presumably caused by the background turbulent fluctuations, a restoring force appears that drives δ back to the stable point. One sees that for the single roll case $\delta^*(\Delta\theta)$ is a straight-line [Fig. 7(a)]. For the LSC in the water layer Fig. 7(b) shows that small wavy variation appears on $\delta^*(\Delta\theta)$ which remains still a continuous function and a stable fixed point always exists for $0 \leq \Delta\theta \leq 2\pi$. Figure 7(c) shows that for LSC in the FC77 layer the intersection line $\delta^*(\Delta\theta)$ turns into unclosed loops surrounding the crests near $\Delta\theta \approx (0, \pi)$. However, near the trough with $\Delta\theta \approx (\pi/2)$ there exists no stable fixed points. It hints that flow cessations and reversals may be prone to occur in this flow state since $\dot{\delta}^d$ remains negative for all values of δ .

Based on Eqs. (8) and (9) we calculate the potential wells $V(\delta) = -\int \dot{\delta}^d(\delta) d\delta$ for the flow strength of the two LSCs. Figures 8(a) and 8(b) depict $V(\delta)$ at various relative orientation ($\Delta\theta = 0, \pi/4, \pi/2$) for the LSC in the FC77 and water layer, respectively. One sees that with increasing $\Delta\theta$ the potential barrier $\Delta V = V(0) - V(\delta_0)$ for the LSC in FC77 layer becomes small gradually. When $\Delta\theta = \pi/2$, the potential barrier eventually disappears and $V(\delta)$ increases monotonically with δ . Within such a repulsive potential, the flow strength δ of the FC77 roll drifts spontaneously towards the stable fixed point $\delta^* = 0$ irrespective of its initial status. In this sense, the FC77 roll is prone to cease in the flow state when the two LSC planes are orthogonal to each other with $\Delta\theta = \pi/2$. We thus suggest that there exist two distinct stochastic dynamic processes through which flow cessations and reversals may occur. Starting from the most probable flow state of thermal coupling ($\Delta\theta = 0$), for example, and with its amplitude being at the bottom of the potential well ($\delta = \delta_0$), the LSC in the FC77 layer acquires stochastic forcing for both degrees of freedom of its temperature amplitude δ and the relative orientation θ . A cessation (or reversal) event occurs when fluctuations in δ cross the potential barrier ΔV and δ drops to zero, while the system remains in a thermal coupling state ($\Delta\theta = 0$). We refer this process as amplitude-fluctuation induced cessation

(reversal), a well-known stochastic process observed in turbulent convection with a single-roll LSC. Flow cessation and reversal events can be also achieved in a two-layer convection system when stochastic fluctuations drive the azimuthal diffusion of two coupling LSCs such that the system switches between various preferred states (e.g., thermal coupling and viscous coupling, etc.). Under the circumstance that the two LSC planes are right-angled to each other ($\Delta\theta \approx \pi/2$), the LSC amplitude of the FC77 roll δ drops to zero momentarily, owing to a deterministic force created by the positive potential $V(\delta, \Delta\theta = \pi/2)$ as depicted in Fig. 8(a). This is an orientation-fluctuation induced cessation (reversal) event which is a new stochastic process observed in the present convection system of two interacting LSCs.

Both our experimental and modeling data shown in Figs. 4(c) and 6(c) reveal that when the flow strength of the FC77 roll is weak (e.g., $\delta/\langle\delta\rangle \approx 0.35$), there is a considerably large possibility to two LSC planes are orthogonal to each other with $\Delta\theta = \pi/2$. It is an evidence that a significant portion of cessation and reversal event of the FC77 roll may occur through the orientation-fluctuation induced process. Indeed, we have observed from our experimental (modeling) data that 27.3 (56.7) percent of cessation events are orientation-fluctuation induced. When the flow state of the two LSCs evolves from thermal coupling or viscous coupling, to a flow configuration that their circulating planes are orthogonal to each other, a momentary vanishing of the FC77 roll occurs, followed by a revival of the LSC flow likely returning to the state of thermal coupling or viscous coupling. The above analysis thus provide a new perspectives into understanding the significantly enhanced frequency of flow cessations and reversals observed in the FC77 layer. In the water layer, however, the potential function $V(\delta)$ of the LSC amplitude is nearly independent of $\Delta\theta$ [Fig. 8(b)]. Hence even in the flow state when the two LSC planes are orthogonal to each other ($\Delta\theta = \pi/2$), cessations and reversals occur only when fluctuations of the LSC amplitude is large enough to overcome the potential barrier that has a similar amplitude. We thus interpret the apparently different stochastic behavior of the two LSCs. Our model provides predictions for the occurrence frequency of flow cessations and reversals which is in good agreements with the experimental observations (Fig. 5).

Figure 9 presents an example of the experimental results of the time series of δ and $\Delta\theta$ when the FC77 roll undergoes a reversal event, displayed over the phase surface $\delta_{FC}(\delta_{FC}/\langle\delta_{FC}\rangle, \Delta\theta)$. Before flow reversal starts, we see that the two LSCs are in a thermal coupling state with $\Delta\theta = 0$ and the strength of the FC77 roll is meandering around the stable position $\delta_{FC}^d \approx \langle\delta_{FC}\rangle$ (see the red part of the trajectory in Fig. 9). The reversal event is initialized when $\Delta\theta$ undergoes an abrupt shift towards $\Delta\theta = \pi/2$, presumably owing to the stochastic force f_{θ} that drives the azimuthal rotation of the FC77 roll, while its flow strength δ_{FC} remains nearly unchanged in this process. When $\Delta\theta$ reaches $\pi/2$, i.e., the circulating planes of the two LSCs are right-angled to each other, δ_{FC} starts to decrease rapidly, reaching a minimum $\delta_{FC} \approx 0.1\langle\delta_{FC}\rangle$ (see the purple part of the trajectory). As we have interpreted in the model, in this flow state the potential $V_{FC}(\delta)$ is positive with a positive slope $\partial V_{FC}(\delta)/\partial\delta > 0$ for all δ_{FC} [see the blue curve in Fig. 8(a)], which promotes the occurrence of cessation and reversal events. When the FC77 roll is at a low level of flow strength $\delta_{FC} \ll \langle\delta_{FC}\rangle$, its angular momentum is small and thus its azimuthal orientation exhibits erratic motions until for this case it reaches $\Delta\theta = \pi$. In this flow state of viscous coupling we see that the flow strength δ_{FC} gradually resumes to its mean value $\langle\delta_{FC}\rangle$ (the blue part of the trajectory) and the reversal event is accomplished. Such sequence of events typifies the evolution of flow states during a reversal event, which occurs relatively frequently in the present two-layer convection system.

V. CONCLUSION

In this paper we propose a low-dimensional model to interpret the rich dynamics of two interacting large-scale circulations in two-layer turbulent thermal convection. Extending previous models for single LSC dynamics in RBC [18,19], our model consists of four stochastic ordinary differential equations to describe the strength δ and azimuthal orientations θ of the two LSCs, with their deterministic terms formulated by volume-average of the momentum terms in the NS equations, given by the empirically known structures of the LSC rolls. The interaction terms of

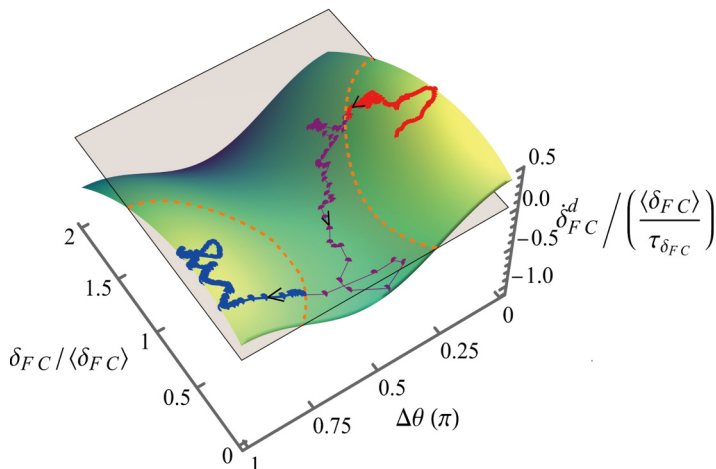


FIG. 9. Experimental results for the time series of δ and $\Delta\theta$ of the FC77 roll which undergoes a flow reversal, overlying the phase surface $\delta_{FC}(\delta_{FC}/\langle\delta_{FC}\rangle, \Delta\theta)$ predicted by the model. The red part of the trajectories represents the meandering movement of the flow strength around the stable position $\langle\delta_{FC}\rangle$ in the state of thermal coupling. The purple line shows the rapid orientational change of the FC77 roll towards the state of viscous coupling, and a momentary vanishing of its flow strength near $\Delta = \pi/2$. After this reversal event, the strength of the FC77 roll gradually resumes at the state of viscous coupling $\Delta\theta = \pi$ as shown by the blue line. The orange dashed line represents the intersection of the phase surface $\delta_{FC}(\delta_{FC}/\langle\delta_{FC}\rangle, \Delta\theta)$ with the plane $\delta = 0$ (indicated by the grey horizontal plane). The black arrows on the trajectory denote the direction of flow-state evolution.

the two vertically aligned LSCs, i.e., thermal and viscous coupling terms, are predicted based on the influence of the fluid temperature induced by the other LSC roll through heat advection and thermal diffusion, and the enhanced (reduced) viscous dissipation across the interface between the two LSC rolls. The effects of the background turbulent fluctuations are represented by stochastic forcing terms for both the δ and θ equations.

Our model produces two stable LSC rolls interacting with each other, and predicts their preferred flow states of thermal and viscous coupling. The model describes properly the diffusive motion of the LSC amplitudes δ in a deterministic potential $V(\delta)$ and predicts accurately the Poissonian distribution of time interval between LSC cessations. More importantly, our study shows that for two vertically aligned, interacting LSCs in turbulent convection, flow reversals and cessations can be initiated when turbulent fluctuations force the stochastic azimuthal motion of the two LSCs into a flow state with the orientation of the two LSC planes being right-angled to each other, the amplitude δ of the LSC in the fluid layer with a relatively larger Ra drops to zero, driven by a deterministic force created in its positive potential $V(\delta, \Delta\theta = \pi/2)$. Flow reversal is achieved when the LSC resumes in the opposite azimuthal position.

Previous studies on the LSC dynamics in turbulent convection have proposed several scenarios for the mechanism of flow reversals. Flow reversals in turbulent RBC are often interpreted as an intrinsic instability of the LSC structure which switches between two bistable states [13,17–19]. Such a flow instability is initialized, either by a transitory imbalance between the buoyancy forcing and viscous damping of the LSC [13,17], or by stochastic fluctuations in the background turbulence [18,19]. Other experiments suggest that LSC reversal may be ascribed to external disturbances from secondary flows. For convection in a quasi two-dimensional domain, flow reversals occur when the corner vortices drain energy from and destabilize the main LSC structure [21,51]. In recent works, the irregular flow reversals and cessations are viewed as a dynamical process of heat accumulation and release in thermal convection [24]: the abrupt massive eruption of thermal plumes,

which releases the accumulated heat in the convective fluid, interrupts the existing LSC and resets its azimuthal direction. While these studies provide perceptive descriptions of LSC reversals in a single-roll configuration, from different viewpoints of experiments and numerical simulations, they suggest different theoretical interpretations of the phenomena.

In the present work we demonstrate that in two-layer turbulent convection the stability of the flow structures depends on the interacting degrees of freedom of the two LSCs. Importantly, the mechanism of flow reversal in this system is underpinned by multiple dynamical processes: a stochastic process that the two LSCs undergo azimuthal diffusion driven by the background turbulent fluctuations and switch randomly between various flow states, and a deterministic process in which the strength of the LSC reduces monotonically owing to a reduction of buoyancy forcing on the LSC structure. The success of our model in predicting the enhanced occurrence frequency of flow reversals and cessations in two-layer convection suggests that the turbulent flow dynamics of interacting large-scale flows can be described by physically based, low-dimensional approximate models. The interactions between two adjacent LSCs, and the resultant stochastic dynamics as elucidated in the present work, may be of fundamental significance for turbulent flows with multiple large-scale structures. Thus the present modeling approach may be applied more generally to multilayer convection systems in which multiple convection rolls coexist and interact thermally and mechanically. Turbulent convection in multiple fluid layers (such as convection in the air-ocean system and in the Earth's fluid core and its mantle) has been a challenging subject for numerical and experimental studies but is of great practical importance. Our work brings insights into understanding the dynamics of these turbulent flows and may inspire further studies.

ACKNOWLEDGMENTS

This work was supported by the National Natural Science Foundation of China under Grants No. 92152105, No. 12174287, No. 92152104, No. 12002260, No. 12072144, and No. 12232010, the Research Program of Science and Technology Commission of Shanghai Municipality, and the Fundamental Research Funds for the Central Universities in China.

Y. Sun, Y.-C. Xie, and J.-X. Xie contributed equally to this study.

APPENDIX: MEASURING THE MODEL PARAMETERS

Our model of two interacting LSCs requires several input parameters. Given by the experimental conditions $\text{Ra}_{\text{FC}} = 1.59 \times 10^{11}$, $\text{Ra}_w = 1.23 \times 10^9$ and $\sigma_{\text{FC}} = 19.6$, $\sigma_w = 8.1$, our measurements of the sidewall temperature show that the mean temperature amplitudes for the LSCs in the FC77 and water are $\delta_{10} = \langle \delta_{\text{FC}} \rangle = 0.21$ K and $\delta_{20} = \langle \delta_w \rangle = 0.57$ K, respectively. The Reynolds numbers of the two LSC are evaluated based on the Grossmann-Lohse theory [50], $\text{Re}_{\text{FC}} = 4446.7$ and $\text{Re}_w = 940.2$.

For a variable x that undergoes diffusive fluctuations, the mean-square displacement $\langle (dx)^2 \rangle$ over a small time interval dt is given by $\langle (dx)^2 \rangle = D_x dt$, where D_x is defined as the diffusivity of x . For a sufficiently large time, $\langle (dx)^2 \rangle = 2\tau_x D_x$ approaches a constant, with τ_x being the characteristic timescale of the diffusive motion. In our model, the stochastic terms $f_x(t)$ are modeled as Gaussian white noise that have a variance of D_x/h , where h is the time step.

Figure 10 shows the mean-square displacements $\langle (d\delta_{\text{FC}})^2 \rangle$ and $\langle (d\delta_w)^2 \rangle$ as functions of the time interval dt . The equation $\langle (d\delta)^2 \rangle = D_\delta dt$ is fitted to both data sets for the FC77 layer and water layer, in the linear range of the time interval $30s \leq dt \leq 90s$, to obtain $D_{\delta_{\text{FC}}} = 0.92 \times 10^{-5}$ K²/s and $D_{\delta_w} = 3.2 \times 10^{-5}$ K²/s. For a sufficiently large time interval $dt \geq 10^3$ s, we use $\langle (d\delta)^2 \rangle = 2\tau_\delta D_\delta$ to determine $\tau_{\delta_{\text{FC}}} = 191$ s and $\tau_{\delta_w} = 84$ s. Following a similar scheme we determine the dynamical parameters for the diffusive motion of θ as follows, $D_{\dot{\theta}_{\text{FC}}} = 0.95 \times 10^{-4}$ K²/s, $\tau_{\dot{\theta}_{\text{FC}}} = 1.8$ s and $D_{\dot{\theta}_w} = 1.1 \times 10^{-5}$ K²/s, $\tau_{\dot{\theta}_w} = 1.2$ s.

Our model contains three unknown parameters a , b , and I_0 to be determined by matching between the experimental data and the modeling outputs. Here we examine the experimental and

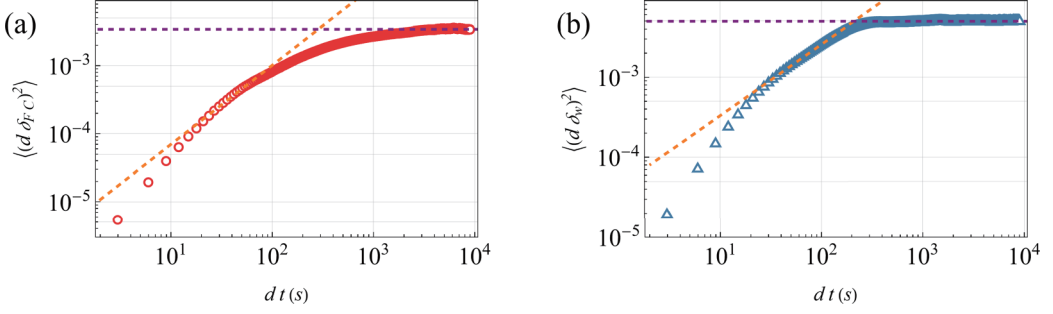


FIG. 10. The mean-square displacements $\langle (d\delta_{FC})^2 \rangle$ (a) and $\langle (d\delta_w)^2 \rangle$ (b) as a function of the time interval dt . The orange dashed lines denote $\langle (d\delta_{FC})^2 \rangle = D_{\delta_{FC}} dt$ and $\langle (d\delta_w)^2 \rangle = D_{\delta_w} dt$ with $D_{\delta_{FC}} = 0.921 \times 10^{-5} \text{ K}^2/\text{s}$ and $D_{\delta_w} = 3.2 \times 10^{-5} \text{ K}^2/\text{s}$. The purple dashed line shows the fitted constant $2D_\delta \tau_\delta$ for large dt , yielding $\tau_{\delta_{FC}} = 191 \text{ s}$ and $\tau_{\delta_w} = 84 \text{ s}$.

modeling results of (i) the PDF of the flow coupling states $p(\Delta\theta)$ as shown in Fig. 3(c), and (ii) the ratio $R(\delta_{FC}) \equiv \int_{-\pi/4}^{\pi/4} p(\Delta\theta) d\Delta\theta / \int_{3\pi/4}^{5\pi/4} p(\Delta\theta) d\Delta\theta$ that reveals the probability whether the LSC in the FC77 layer is in the flow state of thermal coupling or viscous coupling for various flow strength. We calculate the mean-square deviations of the modeling results of these two quantities from the experimental ones, i.e., $\Delta_R^2 = \int_0^{1.4} (R_e - R_m)^2 d\delta_{FC} / \langle \delta_{FC} \rangle$ and $\Delta_P^2 = \int_0^{2\pi} (p_e - p_m)^2 d\Delta\theta$. The subscripts e and m denote data from the experiment and the model, respectively. $\delta_{FC} / \langle \delta_{FC} \rangle = 1.4$ is the maximum value of $\delta_{FC} / \langle \delta_{FC} \rangle$ observed in the experiment. Following the least-square method, we determine the optimal values of the parameters ($a = 0.13$, $b = 0.22$, $I_0 = 1.76$) by setting the quantity $\Delta^2 \equiv \Delta_R^2 / \int_0^{1.4} R_e d\delta_{FC} / \langle \delta_{FC} \rangle + \Delta_P^2 / \int_0^{2\pi} p_e d\Delta\theta$ a minimum.

For demonstration we show in Fig. 11 model results of the ratio R as functions of $\delta_{FC} / \langle \delta_{FC} \rangle$ for three sets of parameters (a , b , and I_0), which are compared with the experimental data. Δ_R^2 for these three sets of result are 6.85 (blue triangles), 40.51 (orange diamonds), and 16.76 (purple squares), respectively. Furthermore, we calculate $p(\Delta\theta)$ using these three sets of parameters to find out $\Delta_P^2 = (1.35, 3.43, 2.44)$, and $\Delta^2 = (0.59, 2.21, 1.19)$. Last, we find that with the combined parameters ($a = 0.13$, $b = 0.22$, $I_0 = 1.76$) the mean-square deviation $\Delta^2 = 0.59$ reaches the

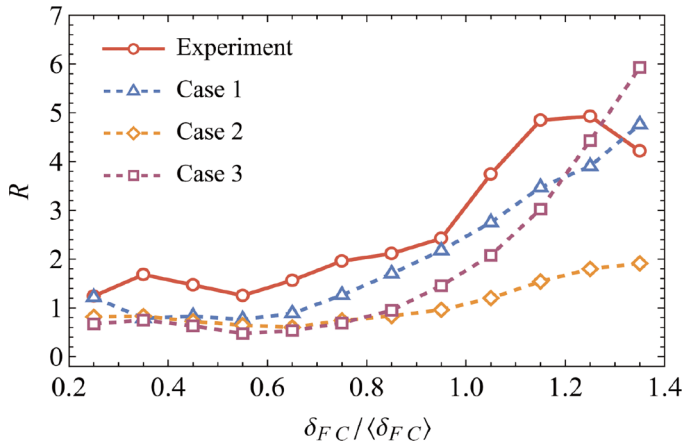


FIG. 11. The ratio R as functions of $\delta_{FC} / \langle \delta_{FC} \rangle$. Red circles (solid line): experimental results. Other symbols (dashed lines): model results using different sets of parameters. Triangles represent the result with the optimal parameters (case 1: $a = 0.13$, $b = 0.22$, $I_0 = 1.76$). Diamonds and squares are results for (case 2: $a = 0.12$, $b = 0.22$, $I_0 = 1.76$) and (case 3: $a = 0.13$, $b = 0.3$, $I_0 = 1.64$), respectively.

global minimum over the parameter range that is explored, and this result determines the optimal parameters for our model.

The values of the main parameters used in the model are presented in Table I.

-
- [1] J. Marschall and F. Scott, Open-ocean convection: Observations, theory, and models *Rev. Geophys.* **37**, 1 (1999).
 - [2] G. Glatzmaier, R. Coe, L. Hongre, and P. Roberts, The role of the Earth's mantle in controlling the frequency of geomagnetic reversals, *Nature (London)* **401**, 885 (1999).
 - [3] P. Olson, Experimental dynamos and the dynamics of planetary cores, *Annu. Rev. Earth Planet. Sci.* **41**, 153 (2013).
 - [4] M. Miesch, The coupling of solar convection and rotation, *Sol. Phys.* **192**, 59 (2000).
 - [5] R. K. Yadav, M. Heimpel, and J. Bloxham, Deep convection-driven vortex formation on jupiter and saturn, *Sci. Adv.* **6**, eabb9298 (2020).
 - [6] F. M. Richter and C. E. Johnson, Stability of a chemically layered mantle, *J. Geophys. Res.* **79**, 1635 (1974).
 - [7] A. Prakash and J. N. Koster, Convection in multiple layers of immiscible liquids in a shallow cavity I. steady natural convection, *Int. J. Multiphase Flow* **20**, 383 (1994).
 - [8] G. Ahlers, S. Grossmann, and D. Lohse, Heat transfer and large-scale dynamics in turbulent Rayleigh-Bénard convection, *Rev. Mod. Phys.* **81**, 503 (2009).
 - [9] D. Lohse and K.-Q. Xia, Small-scale properties of turbulent Rayleigh-Bénard convection, *Annu. Rev. Fluid Mech.* **42**, 335 (2010).
 - [10] F. Chillà and J. Schumacher, New perspectives in turbulent Rayleigh-Bénard convection, *Eur. Phys. J. E* **35**, 58 (2012).
 - [11] R. Krishnamurti and L. N. Howard, Large-scale flow generation in turbulent convection, *Proc. Natl. Acad. Sci. USA* **78**, 1981 (1981).
 - [12] J. J. Niemela, K. R. Skrbek, L. and Sreenivasan, and R. J. Donnelly, The wind in confined thermal convection, *J. Fluid Mech.* **449**, 169 (2001).
 - [13] K. R. Sreenivasan, A. Bershadskii, and J. J. Niemela, Mean wind and its reversal in thermal convection, *Phys. Rev. E* **65**, 056306 (2002).
 - [14] D. Funfschilling and G. Ahlers, Plume motion and large-scale circulation in a cylindrical Rayleigh-Bénard cell, *Phys. Rev. Lett.* **92**, 194502 (2004).
 - [15] E. Brown, A. Nikolaenko, and G. Ahlers, Reorientation of the large-scale circulation in turbulent Rayleigh-Bénard convection, *Phys. Rev. Lett.* **95**, 084503 (2005).
 - [16] R. Benzi, Flow reversal in a simple dynamical model of turbulence, *Phys. Rev. Lett.* **95**, 024502 (2005).
 - [17] F. F. Araujo, S. Grossmann, and D. Lohse, Wind reversals in turbulent Rayleigh-Bénard convection, *Phys. Rev. Lett.* **95**, 084502 (2005).
 - [18] E. Brown and G. Ahlers, Large-scale circulation model for turbulent Rayleigh-Bénard convection, *Phys. Rev. Lett.* **98**, 134501 (2007).
 - [19] E. Brown and G. Ahlers, A model of diffusion in a potential well for the dynamics of the large-scale circulation in turbulent Rayleigh-Bénard convection, *Phys. Fluids* **20**, 075101 (2008).
 - [20] H.-D. Xi, S.-Q. Zhou, Q. Zhou, T.-S. Chan, and K.-Q. Xia, Origin of the temperature oscillation in turbulent thermal convection, *Phys. Rev. Lett.* **102**, 044503 (2009).
 - [21] K. Sugiyama, R. Ni, R. J. A. M. Stevens, T. S. Chan, S. Q. Zhou, H. D. Xi, C. Sun, S. Grossmann, K.-Q. Xia, and D. Lohse, Flow reversals in thermally driven turbulence, *Phys. Rev. Lett.* **105**, 034503 (2010).
 - [22] J.-Q. Zhong, S. Sterl, and H.-M. Li, Dynamics of the large-scale circulation in turbulent Rayleigh-Bénard convection with modulated rotation, *J. Fluid Mech.* **778**, R4 (2015).
 - [23] J.-Q. Zhong, H.-M. Li, and X.-Y. Wang, Enhanced azimuthal rotation of the large-scale flow through stochastic cessations in turbulent rotating convection with large Rossby numbers, *Phys. Rev. Fluids* **2**, 044602 (2017).

- [24] Y. Wang, P.-Y. Lai, H. Song, and P. Tong, Mechanism of large-scale flow reversals in turbulent thermal convection, *Sci. Adv.* **4**, eaat7480 (2018).
- [25] D.-D. Ji, K. Bai, and E. Brown, Effects of tilt on the orientation dynamics of the large-scale circulation in turbulent Rayleigh–Bénard convection, *Phys. Fluids* **32**, 075118 (2020).
- [26] E. Brown and D. Ji, Interactions between two adjacent convection rolls in turbulent Rayleigh–Bénard convection, *Phys. Rev. Fluids* **8**, 064608 (2023).
- [27] U. Hansen, D. A. Yuen, and S. E. Kroening, Mass and heat transport in strongly time-dependent thermal convection at infinite Prandtl number, *Geophys. Astrophys. Fluid Dyn.* **63**, 67 (1992).
- [28] E. Brown and G. Ahlers, Rotations and cessations of the large-scale circulation in turbulent Rayleigh–Bénard convection, *J. Fluid Mech.* **568**, 351 (2006).
- [29] S. Cioni, S. Ciliberto, and J. Sommeria, Strongly turbulent Rayleigh–Bénard convection in mercury: comparison with results at moderate Prandtl number, *J. Fluid Mech.* **335**, 111 (1997).
- [30] H.-D. Xi and K.-Q. Xia, Cessations and reversals of the large-scale circulation in turbulent thermal convection, *Phys. Rev. E* **75**, 066307 (2007).
- [31] Resagk, R. du Puits, A. Thess, F. V. Dolzhansky, S. Grossmann, F. Fontenele Araujo, and D. Lohse, Oscillations of the large-scale wind in turbulent thermal convection, *Phys. Fluids* **18**, 095105 (2006).
- [32] H.-D. Xi and K.-Q. Xia, Flow mode transitions in turbulent thermal convection, *Phys. Fluids* **20**, 055104 (2008).
- [33] S. Weiss and G. Ahlers, Heat transport by turbulent rotating Rayleigh–Bénard convection and its dependence on the aspect ratio, *J. Fluid Mech.* **684**, 407 (2011).
- [34] K. Petschel, M. Wilczek, M. Breuer, R. Friedrich, and U. Hansen, Statistical analysis of global wind dynamics in vigorous Rayleigh–Bénard convection, *Phys. Rev. E* **84**, 026309 (2011).
- [35] E. P. van der Poel, R. J. A. M. Stevens, K. Sugiyama, and D. Lohse, Flow states in two-dimensional Rayleigh–Bénard convection as a function of aspect-ratio and Rayleigh number, *Phys. Fluids* **24**, 085104 (2012).
- [36] S. Wagner and O. Shishkina, Aspect-ratio dependency of Rayleigh–Bénard convection in box-shaped containers, *Phys. Fluids* **25**, 085110 (2013).
- [37] M. Bukai, A. Eidelman, T. Elperin, N. Kleeorin, I. Rogachevskii, and I. Sapir-Katiraie, Effect of large-scale coherent structures on turbulent convection, *Phys. Rev. E* **79**, 066302 (2009).
- [38] J. Verdoodt, M. J. Tummers, and K. Hanjalić, Oscillating large-scale circulation in turbulent Rayleigh–Bénard convection, *Phys. Rev. E* **73**, 056304 (2006).
- [39] Q. Wang, Z. H. Wan, R. Yan, and D. J. Sun, Multiple states and heat transfer in two-dimensional tilted convection with large aspect ratios, *Phys. Rev. Fluids* **3**, 113503 (2018).
- [40] D. Ji, Modeling of the dynamics of large-scale coherent structures in the system of Rayleigh–Bénard Convection, Ph.D. thesis, Yale University, 2019.
- [41] Y.-C. Xie and K.-Q. Xia, Dynamics and flow coupling in two-layer turbulent thermal convection, *J. Fluid Mech.* **728**, R1 (2013).
- [42] H.-R. Liu, K. L. Chong, R. Yang, R. Verzicco, and D. Lohse, Heat transfer in turbulent Rayleigh–Bénard convection through two immiscible fluid layers. *J. Fluid Mech.* **938**, A31 (2022).
- [43] H.-R. Liu, K. L. Chong, Q. Wang, C. S. Ng, R. Verzicco, and D. Lohse, Two-layer thermally driven turbulence: Mechanisms for interface breakup, *J. Fluid Mech.* **913**, A9 (2021).
- [44] Y.-C. Xie, P. Wei, and K.-Q. Xia, Dynamics of the large-scale circulation in high-Prandtl-number turbulent thermal convection, *J. Fluid Mech.* **717**, 322 (2013).
- [45] G. Ahlers, E. Brown, and A. Nikolaenko, The search for slow transients, and the effect of imperfect vertical alignment, in turbulent Rayleigh–Bénard convection, *J. Fluid Mech.* **557**, 347 (2006).
- [46] S. Grossmann and D. Lohse, Prandtl and Rayleigh number dependence of the Reynolds number in turbulent thermal convection, *Phys. Rev. E* **66**, 016305 (2002).
- [47] E. Brown and G. Ahlers, Effect of the Earth’s Coriolis force on the large-scale circulation of turbulent Rayleigh–Bénard convection, *Phys. Fluids* **18**, 125108 (2006).
- [48] X.-L. Qiu and P. Tong, Large-scale velocity structures in turbulent thermal convection, *Phys. Rev. E* **64**, 036304 (2001).

- [49] X.-L. Qiu and P. Tong, Onset of coherent oscillations in turbulent Rayleigh-Bénard convection, [Phys. Rev. Lett. **87**, 094501 \(2001\)](#).
- [50] S. Grossmann and D. Lohse, Thermal convection for large Prandtl numbers, [Phys. Rev. Lett. **86**, 3316 \(2001\)](#).
- [51] D. P. Wang X. Chen and H. D. Xi, Reduced flow reversals in turbulent convection in the absence of corner vortices, [J. Fluid Mech. **891**, R5 \(2020\)](#).